Unusual behaviour of Au/ZnO catalysts in selective hydrogenation of butadiene due to the formation of a AuZn nanoalloy

Salim Derrouiche, Camille La Fontaine, Gode Thrimurtulu, Sandra Casale, Laurent Delannoy, Hélène Lauron-Pernot, Catherine Louis

Unusual behaviour of Au/ZnO catalysts in selective hydrogenation of butadiene due to the formation of AuZn nanoalloy

Salim Derrouiche[1,2], Camille La Fontaine[1,2], Gode Thrimurtulu[1,2], Sandra Casale[1,2], Laurent Delannoy[1,2], Hélène Lauron-Pernot[1,2], Catherine Louis[1,2 *]

[1] *Sorbonne Universités, UPMC Univ Paris 06, UMR 7197, Laboratoire de Réactivité de Surface, 4 Place Jussieu, F-75005, Paris, France*

[2] *CNRS, UMR 7197, Laboratoire de Réactivité de Surface, 4 Place Jussieu, F-75005, Paris, France*

* Corresponding author: catherine.louis@upmc.fr

Abstract

The reaction of selective hydrogenation of butadiene performed in an excess of propene, which has been extensively studied over gold supported on different oxides and exhibited high selectivity to butenes, has been applied to the case of gold (1 wt%) supported on zinc oxide (8 m^2/g), a strongly basic oxide, in order to try to thwart deactivation. Our results revealed for the first time, a catalytic behaviour drastically different from what was observed over gold catalysts supported on alumina or titania, i.e., a much poorer activity when the catalyst was activated in usual conditions under hydrogen but a "normal" activity when it was activated in air. An in-depth characterisation study based on different hypotheses to explain the unusual result, revealed that at variance with the other catalysts, Au_1Zn_1 alloyed particles formed during activation under hydrogen at 300 °C, and were responsible for the loss of activity.

1. Introduction

Au/ZnO catalysts are the focus of recent catalytic studies involving chemical energy storage and green technologies. One can cite the recent paper of Hartadi et al. [1] on CO_2 hydrogenation to methanol, the one of Ke et al. [2] on oxidative esterification of ethylene glycol into methanol and also the one of Wu et al. [3] on total oxidation of aromatic-based molecules. In these papers, gold nanoparticles (NPs) were supported on different oxide supports, and Au/ZnO was found to provide the best performances. Au/ZnO has been also reported as an efficient catalyst for methanol steam reforming for hydrogen and CO_2 production [4], for carbon monoxide hydrogenation into methanol [5], for CO oxidation [6-8] and for CO oxidation in excess of H_2 (PROX reaction) [9-10]. Moreover, Au/ZnO has been also used as photocatalysts under UV and/or visible irradiation for photodegradation of dyes in liquid phase [11-13], and of benzene in gas phase [14].

On the other hand, the reaction of selective hydrogenation of butadiene performed in an excess of propene (propene/butadiene ratio =100) is an important model reaction that has been developed in our laboratory to mimic the process of catalytic purification of alkene cuts from impurities of dienes or alkynes, and especially of butene cuts (for analytical reason, butene is replaced by propene). This reaction has been extensively studied over oxide-supported gold catalysts in temperature programmed reaction from RT to 300 °C [15-16]. Even though gold catalysts are not very active in hydrogenation reaction, these previous works revealed their very high selectivity to butenes, even in presence of an excess of propene. At the temperature corresponding to 100% conversion ($T_{100\%}$), i.e. around 160 °C under our reaction conditions, butadiene was transformed only into butenes (1-butene, *trans*-2-butene and *cis*-2-butene) without formation of any alkanes (butane or propane). This reaction was found very sensitive (i) to the gold particle size; activity decreased as the particle size increased but the TOF was constant, indicating the reaction was not structure sensitive; (ii) to

the presence of chlorides, which inhibit the reaction [15]; (iii) to the addition of a second metal, such as Pd, that induced a positive effect on the activity with almost no effect on selectivity provided that the Au/Pd atomic ratio remained higher than 20 [17]. In contrast, no influence of the nature of the oxide support on the activity and selectivity was found among those tested: alumina, titania, ceria, zirconia, indicating that the reaction takes place only on the metal particles [15]. However, deactivation was observed [15], and seems to depend on the acid-base properties of the support as deactivation was stronger for acidic supports such as alumina, than for non acidic (zirconia) and basic supports (ceria).

Considering the interesting catalytic properties of Au/ZnO enounced above and the fact that zinc oxide is strongly basic and could reduce deactivation, we decided to prepare Au/ZnO catalysts using the same preparation method as for the other gold catalysts cited above, i.e., deposition-precipitation with urea, and to test them in selective hydrogenation of butadiene. It seems that this preparation method has never been used before for the preparation of Au/ZnO; deposition-precipitation with urea allows to deposit the whole gold from the solution, to limit the amount of chlorides coming from the gold precursor, $HAuCl_4$, and to lead to the formation of small particles after reduction (2-3 nm) [15, 17-19]. The so-prepared Au/ZnO catalysts were tested under the same conditions as in previous works [15-17], i.e., after the same *in situ* activation treatment under hydrogen at 300 °C and under the same conditions of reaction. Amazingly for the first time, a gold catalyst supported on oxide, Au/ZnO, behaved drastically differently, and this led us to characterise the samples in-depth and to investigate different hypotheses to explain this peculiar behaviour.

2. Experimental

2.1. Au/ZnO catalyst preparation

1 wt% Au/ZnO catalyst was prepared by deposition-precipitation with urea (DPU) according to the procedure described elsewhere [18-19], using $HAuCl_4$ as gold precursor and ZnO Kadox-911 from Horsehead as support; its BET surface area was 8 $m^2.g^{-1}$ after a treatment in oxygen at 400 °C for 2 h. Briefly, 2 g of ZnO were mixed to 200 mL of aqueous solution containing the appropriate amount of $HAuCl_4.3H_2O$ in order to achieve the desired nominal gold loading of 1 wt%. Urea was added to achieve a urea to metal molar ratio of 100. The mixture was stirred in the dark at 80 °C in a closed reactor for 16 h. The solid was separated from the liquid by centrifugation and subsequently repeatedly washed with distilled water and repeatedly centrifuged (four times). The sample was further dried under vacuum at room temperature (RT) for 24 h (as-prepared samples).

The as-prepared sample was then stored in a desiccator under vacuum at RT and in the dark. Chemical analysis showed that the Au/ZnO sample contained 0.90 wt% Au and 400 ppm Cl.

Before characterization or reaction, the catalysts were thermally treated at 300 °C for 2 h after a temperature ramp of 2 °C.min^{-1} under a flow (100 mL.min^{-1}) of either pure H_2 (so-called reduction) or air (so-called calcination). Note that, for most of the oxide supports, gold was reduced in the metallic state in both cases.

2.2. Techniques

Chemical analysis of Au in the as-synthesized samples was performed by inductively coupled plasma atom emission spectroscopy at the CNRS Center of Chemical Analysis (Vernaison, France).

Temperature programmed reduction (TPR) was performed using a Micromeritics Autochem II Automated Catalyst Characterization System by passing 5% H_2/Ar gas mixture (25 mL.min^{-1}) through the catalyst (200 mg) while increasing the temperature at a linear rate (7.5 °C.min^{-1}) from RT to 850 °C.

The XRD data were recorded on a diffractometer (D8 Bruker) using the Cu-Kα radiation (1.5418 Å; 40 kV and 30 mA) with a Ni filter. The diffractograms were standardized relatively to the (202) peak at 2θ = 76.99° of pure ZnO. High Resolution XRD was also performed at the University of South Carolina on a Rigaku Miniflex-II using a silicon strip detector (D/teX Ultra) and Cu-Kα radiation (15 kV and 30 mA).

Gold particle size measurements were performed by Transmission Electron Microscopy using a JEOL JEM-100 CX II microscope operating at 100 kV. At least 300 particles were measured one by one using ImageJ software. The size limit for the detection of gold particles on ZnO was *ca.* 1 nm. The average metal particle sizes d_{Au} were expressed as the volumic mean, $d_{Au} = \sum n_i d_i^3 / \sum n_i d_i^2$ and where n_i is the number of particles of diameter d_i. In addition, high resolution imaging was performed using a JEOL LaB_6 JEM-2010 microscope operating at 200 kV.

XPS spectra were collected on a SPECS (Phoibos 100-5 MCD) X-ray photoelectron spectrometer, using a monochromated Al Kα ($h\nu$ = 1486.6 eV) X-ray source. After data collection, the binding energies were calibrated with respect to the C-C/C-H components of the C 1s peak (binding energy = 284.6 eV). All spectra processing was carried out using the Casa XPS software package.

CO adsorption coupled with Diffuse Reflectance Infrared Fourier Transform Spectroscopy (DRIFTS) was performed with a VECTOR 22 Bruker spectrometer using a DRIFTS cell (collector from Spectratech). The sample compartment of the cell was filled with the as-prepared sample (~20 mg), which was heated *in situ* under a flow (50 cm^3.min^{-1}) of

either 5% v/v H_2 in Ar or 20% v/v O_2 in He up to 300 °C with a ramp of 2 °C.min^{-1} followed by a 2 h-plateau at 300 °C. Then the cell was cooled down to RT and purged with He, before the introduction of a flow (50 cm^3.min^{-1}) of 1% v/v CO in He. The first spectrum recorded under He was used as reference, and the intensity of the spectrum recorded under CO/He was expressed as $\log\left(\frac{1}{R'}\right)$ where the relative reflectance R' is given by: $R' = \frac{R}{R_{\infty}} = \frac{I_{CO/He}}{I_{He}}$.

The reaction of selective hydrogenation of butadiene in excess of propene was carried out with 100 mg of catalyst (sieve fraction, 125-200 μm) in a plug flow microreactor (4 mm of internal diameter) in conditions of temperature-programmed reaction. The catalysts were activated *in situ* either under pure H_2 (100 mL.min^{-1}) or air (100 mL.min^{-1}) from RT to 300 °C (2 °C.min^{-1}) and hold for 2 h at the final temperature. Then, the reactor was cooled down under H_2 to RT, and the reaction mixture consisting of 0.3% butadiene, 30% propene and 20% hydrogen in He was introduced with a total flow rate of 50 mL.min^{-1}. The catalysts were heated under this gas mixture at a rate of 1 °C.min^{-1}, from 30 °C up to 300 °C. The analysis of the reaction products was performed by gas chromatography (Perichrom PR 2100, FID detector) every 15 min, thus every 15 °C. As mentioned in ref. [15], tests were made to attest that under the catalytic conditions described and at low conversion, internal and external diffusion limitations could be neglected.

CO oxidation was performed using a flow-type packed-bed reactor at 25 °C, with the reactor immersed in a water bath, and at atmospheric pressure with a feed of 1% CO and 9% O_2 in He (total flow rate 150 mL.min^{-1}; total gas space velocity = 180,000 mL.$g_{catalyst}^{-1}$.h^{-1}). All the reactants employed in this study were of high purity (2%CO in He (99.999%); O_2 (99.995%, H_2O < 3 ppm); He (99.999%, H_2O < 3 ppm). The reaction was performed after *in situ* activation of the gold catalysts (50 mg) with O_2 (20% in He) (100 mL.min^{-1}) at 300 °C or H_2 (100 mL.min^{-1}) at 300 °C. After activation and cooling down to RT under the same gases, the reactor was flushed with He at RT, and replaced by the reaction mixture. The CO

consumption and CO_2 production were monitored using a Varian Micro GC QUAD CP4900 equipped with two analysis channels (Molsieve 5A and Poraplot Q). Catalytic activities, measured at RT for conversions lower than 45%, is expressed as the specific rate in $mol_{CO}.s^{-1}.mol_{Au}^{-1}$.

3. Main Results obtained with the Au/ZnO catalysts

3.1. Gold particle sizes

Figure 1a shows the TPR profile of the as-prepared Au/ZnO sample. A main peak at 160 °C that can be attributed to the reduction of gold is visible, as well as several other smaller peaks; a shoulder at 200 °C, a peak at 260 °C, a broad one around 380 °C, and two other ones at 460 and 510 °C, probably due to ZnO surface reduction, as attested by the TPR profile of ZnO (Figure 1b).

In the following, Au/ZnO has been thermally treated up to 300°C in order to ensure complete gold reduction. Figure 2 reports typical TEM images of the Au/ZnO sample obtained after either reduction (Fig. 2A) or calcination (Fig. 2B) and the corresponding histograms of particle size distribution. The average size of the gold particles is below 3 nm (volumic mean), which is small in spite of the low surface area of ZnO (8 m^2/g) and similar to those obtained on other oxide supports of much higher surface area, such as titania (50 m^2/g) or alumina (100 m^2/g) with the same gold loading of 1 wt% [15] (Table 1). However, at variance with these oxide supports [20-21], the gold particles on zinc oxide were slightly smaller after calcination than after reduction. Chen et al [22] also observed small Au NPs of 1.6 nm for $Au/ZnO/TiO_2$ (0.6 wt% Au in 5 wt% ZnO on TiO_2) prepared by deposition-precipitation with

NH_3 then calcined at 180 °C. They also noted that the addition of ZnO on TiO_2 resulted in higher gold particle dispersion and narrower particle size distribution.

Most of the TEM images show that the gold particles are located on the basal faces of the ZnO particles when the latter exhibit rod-like shape. This was also observed by Kundu et al. [23] in a Au/ZnO sample (3.4 wt% Au) resulting from the deposition of Au NPs synthesized in liquid phase under microwave irradiation in the presence of ZnO nano-rods. The authors mentioned that the Au NPs were preferentially located on the polar faces, i.e., on the Zn-terminated and O-terminated (0001) faces of ZnO. Flytzani et al [24] also observed gold particles of 1–3 nm on ZnO in samples prepared by deposition-precipitation with $NaCO_3$ at pH 8.5 and calcined at 280 °C, and located either at the ends of the ZnO nanorods or on the ZnO (0001) faces of ZnO polyhedra.

3.2. Catalytic behaviour in Hydrogenation of 1,3-butadiene

These samples were tested in the reaction of selective hydrogenation of butadiene in excess of propene (propene/butadiene ratio =100). It was first checked that the ZnO support alone pretreated under the usual conditions of activation under H_2 at 300 °C did not show any activity over the whole range of temperature investigated, from RT to 300 °C. When Au/ZnO was activated under the same conditions, a unusual catalytic behaviour was observed (Figure 3A): the butadiene conversion never reached 100% within the whole temperature range; a maximum butadiene conversion of 60% was obtained at 255 °C, and remained unchanged up to 300 °C. In contrast, when the same as-prepared Au/ZnO sample was activated in air at 300°C (Figure 3B), it exhibited the same classical catalytic behaviour as other gold catalysts, such as Au/Al_2O_3 and Au/TiO_2, containing the same gold loading and gold particles of almost the same size [15, 25], i.e., a $T_{100\%}$ at 160-180 °C with 100% selectivity to butenes, almost no propane formed (200 ppm, which corresponds to 0.07% propene conversion) and roughly the

same proportions into the different butenes (1-butene > 2*cis*-butene ~ 2*trans*-butene) and at 300 °C less than 1000 ppm of alkanes produced. The very atypical catalytic behaviour of the reduced Au/ZnO catalyst was never observed previously, and the issue was obviously to understand why such a difference in catalytic behaviour was observed between the reduced and the calcined Au/ZnO samples.

Since Au/ZnO is also a catalyst active in oxidation reactions, and especially in CO oxidation [6-10], calcined Au/ZnO and reduced Au/ZnO were also tested in this reaction at RT (Figure 4). In both cases, the catalyst was active, but the reduced one (Figure 4Aa) was found twice as less active as the oxidised one (Figure 4Ba). Moreover, when after reduction and CO oxidation, Au/ZnO was calcined, its activity increased (Figure 4Ab), and symmetrically when after calcination and CO oxidation, Au/ZnO was reduced, its activity turned very low (Figure 4Bb), and a further calcination treatment restored the activity (Figure 4Bc) at the same level as the reduced then calcined sample (Figure 4Ab).

To explain these unusual catalytic behaviours, three hypotheses were investigated:

- The hypothesis of a support effect resulting from the formation of oxygen vacancies during the reduction treatment;
- The hypothesis of gold nanoparticles encapsulation by ZnO during reduction;
- The hypothesis of a change in particle structure/composition.

Experiments were then conducted to investigate these three hypotheses.

4. Investigation of the origin of the unusual catalytic behaviour of the reduced Au/ZnO catalyst

4.1. Hypothesis of a support effect

The hypothesis of a support effect, i.e., that oxygen vacancies formed during reduction at the surface of ZnO have a negative influence on the catalytic activity of Au/ZnO, in selective hydrogenation of butadiene, was first considered. It is indeed established that a reducing thermal treatment induces the formation of oxygen vacancies at the surface of ZnO [26]. To determine whether these vacancies are responsible for the poor catalytic activity, we attempted to fill back the vacancies by exposure to oxygen, and noted whether the sample recovered activity. Since oxygen vacancies can be filled by exposure to air at RT [27], after Au/ZnO activation under H_2 at 300 °C and cooling down to RT, the sample was exposed to dry air for 1 or 24 h; the catalytic behaviour of Au/ZnO did not improve in either case (Figure 3C). Even if exposure to air at RT was not able to refill all of the oxygen vacancies, the fact that the catalytic activity remained as low as when the reaction was performed directly after H_2 treatment (Figure 3A), is a convincing indication that the formation of oxygen vacancies during reduction treatment is not responsible for the poor Au/ZnO activity, and that modification of the support is not a key factor. This conclusion is also consistent with our previous study [15] that showed that the catalytic properties of gold catalysts (activated under H_2 at 300 °C) in selective hydrogenation of butadiene were not dependent upon the nature of the oxide support (alumina, titania, zirconia and ceria), i.e., whether the support is able to generate oxygen vacancies or not (for the same gold loading and particles size).

4.2. Hypothesis of gold nanoparticles encapsulation by ZnO

Since ZnO is a reducible support like TiO_2, the hypothesis of an encapsulation of the gold nanoparticles by partially reduced zinc oxide species during the reductive thermal treatment, i.e., the establishment of strong metal support interaction (SMSI) effect, was worth to be investigated. The SMSI effect introduced by Tauster et al. in 1978 [28] is characterized by a strong alteration in the physical and chemical properties of metal particles supported on reducible oxides. The SMSI effect has been extensively studied and often observed for group VIII precious metals over reducible support materials such as TiO_2, V_2O_5, and Nb_2O_5 after reduction at temperature higher than 300 °C. It is generally accepted that partial reduction of support is a prerequisite for encapsulation to occur, consequently altering the chemical properties and the catalytic performances of the metal/oxide systems.

This hypothesis was investigated through the examination of HRTEM images of Au/ZnO reduced at 300 °C. We could not observe any coverage of the Au particles by ZnO layers or particles (Figure 5A). It was worth to examine also the samples after calcination, as encapsulation of gold nanoparticles by ZnO was observed by Liu et al [29] by HRTEM on Au/ZnO nanorods after calcination at 300 °C. They observed zinc oxide onto the top surfaces of the gold nanoparticles. We could not observe any overlayer around the gold particles in our calcined sample (Figure 5B); this is consistent with the fact that the calcined Au/ZnO sample was as active in butadiene hydrogenation as any other gold catalysts, for instance as gold supported on a non reducible oxide like alumina.

4.3. Hypothesis of a change in the particle structure/composition

The third hypothesis was that the gold particles could be modified by zinc during reduction. This hypothesis originates from the fact that in one of our former study on Cu/ZnO catalysts also prepared by DPU [30], we discovered that when the temperature of hydrogen

treatment was high enough (350 °C), the metallic particles did not consist of pure Cu^0 any longer but of Cu_3Zn alloy. For this reason, we attempted to characterise the gold NPs in Au/ZnO after reduction and after calcination using X-ray Diffraction. As the particles were too small to give diffraction peaks using a conventional diffractometer, a high-resolution diffractometer was employed. Figure 6 compares the HR-XRD patterns of Au/ZnO after calcination at 300 °C (Figure 6a) and after reduction at 300 °C (Figure 6b). In spite of the fact that the diffraction peaks are very weak, on the diffractogram of the calcined sample (Figure 6a), one can clearly see the characteristic peaks of Au^0 at 38.2 and 44.4°. In the diffractogram of the reduced sample (Figure 6b), these peaks have disappeared, and a new peak can be observed at 40.3°; After comparison with the JCPDS files of different AuZn alloys, we found that the peak at 40.3° corresponded to the most intense one of the Au_1Zn_1 alloy (JCPDS #72-5425 or #30-0608). The absence of the characteristic peaks of Au^0 in the diffractogram of the reduced sample seems to indicate that all of the gold was involved in the nanoalloy. The main peak of Au_1Zn_1 alloy and other of lower intensity are clearly visible in the diffractogram of a Au/ZnO sample containing larger particles (Figure 7). This sample was prepared by impregnation (1 wt% Au), and after calcination at 500 °C then reduction at 300 °C, the Au_1Zn_1 particles were large enough to be detectable by classical XRD (Figure 7). In addition, this sample was submitted to a further thermal treatment in air at increasing temperature (2 $°C.min^{-1}$ up to the different temperatures reported in Figure 7 and by 1 h plateau). One can see that the Au_1Zn_1 peaks decreased when the air treatment temperature increased; the main one was still visible after calcination at 200 and 250 °C, but disappeared at 300°C while the peaks of Au^0 appeared and continued to grow up with temperature. These results indicate the reversible formation of Au_1Zn_1 during the reduction under H_2 at 300°C.

It may be noted that HR-TEM analysis of several metal particles through their Fourier transform did not permit to distinguish Au_1Zn_1 from Au° because the inter-reticular distance

measured was around 2.3 Å whether the sample was reduced or calcined, thus it could be assigned to the (111) line of either Au_1Zn_1 (2.22-2.26 Å) or Au (2.36 Å). The formation of the Au_1Zn_1 alloy could also explain that the gold metal particles are unusually slightly larger after reduction than after calcination (Table 1 and Figure 2) because of the insertion of Zn atoms in the Au particles.

4.4. Possible origin of the unusual catalytic behaviour of the reduced Au/ZnO catalyst

To summarize, the investigation of the three hypotheses above led to the conclusion that the formation of Au_1Zn_1 alloy is the most plausible reason that explains the unusual catalytic behaviour of the reduced Au/ZnO sample in selective hydrogenation of butadiene. To attempt to explain the reason for the alteration of the catalytic properties when the Au_1Zn_1 alloy forms, the surface properties of Au/ZnO catalyst were also investigated by XPS and DRIFTS coupled with CO adsorption.

5. Characterisation of the surface metal particles

XPS experiments were therefore performed on Au/ZnO after calcination or reduction at 300 °C. As the peaks of Zn $3p_{3/2}$ and Zn $3p_{1/2}$ (at 88.3 and 91.3 eV, respectively) overlap with that of Au $4f_{5/2}$ around 87.5 eV, we focussed on the Au $4f_{7/2}$ peak (Figure 8). No difference in the Au $4f_{7/2}$ binding energy could be observed between Au/ZnO calcined at 300 °C (Figure 8a) and Au/ZnO reduced at 300 °C (Figure 8b): 83.3 and 83.2 eV, respectively. As already reported in several papers [31-34], the binding energies of gold in nanoparticles are lower than the ones of pure Au foil (84 eV for Au $4f_{7/2}$) [35].

To complement the XPS measurements, the surface of the metal particles was probed by CO adsorption coupled with DRIFT spectroscopy (Figure 9). After *in situ* calcination or reduction at 300 °C, the Au/ZnO sample was cooled down to RT in He, then CO (1% in He)

was introduced. The first spectrum recorded just after CO admission over the calcined sample showed a single CO vibration band at 2107 cm^{-1} (Figure 9A). Progressively, this band decreased in intensity under the CO flow while another one at lower frequency (2075 cm^{-1}) increased and stabilized. On Figure 9A, one can also clearly see an isobestic point that indicates that the species corresponding to the band at 2107 cm^{-1} transforms into the one at 2075 cm^{-1}. After stabilization after around 2 h and a half under CO, the band at 2107 cm^{-1} was still slightly more intense than the one at 2075 cm^{-1}, and no band shifts were observed.

In the case of the reduced Au/ZnO sample (Figure 9B), the same trends were observed, i.e., the high frequency band decreased while the low frequency one increased until stabilization after about 3 h. However, the band frequencies were slightly lower, 2101 and 2071 cm^{-1}, and the spectra were significantly much less intense than those of the oxidized sample, as clearly evidenced by the comparison of the first spectrum recorded under CO of the calcined (black line) and reduced samples (red line) in Figure 9C. After spectrum stabilization under CO (Figure 9B), the band at 2101 cm^{-1} has almost completely disappeared while the one at 2071 cm^{-1} has become much more intense than initially, reaching roughly the same intensity as the band at 2075 cm^{-1} of the last spectrum of the calcined sample (Figure 9D).

In reference with previous IR studies performed on various gold systems, Au/TiO_2, Au/Fe_2O_3 and Au/SiO_2, the carbonyl band at 2107/2101 cm^{-1} can be attributed to CO adsorbed on low coordinated surface Au^0 atoms [36-37] (note that CO does not adsorb on flat surface of gold) while the band at 2075/2071 cm^{-1} can be assigned to CO adsorbed on negatively charged gold sites ($Au^{\delta-}$) [36, 38]. Note that Muhler et al. also reported in a transmission IR study [8], the presence of the same bands on Au/ZnO with the same assignments although the band at 2106 cm^{-1} was observed at 110 K and was shifted to 2115 cm^{-1} at 160 K, while the band at 2077 cm^{-1} was observed at 110 K and unstable above 140 K.

The growth of the low frequency band ($Au^{\delta-}$–CO) at the expense of the high frequency one (Au^{0} –CO) could be explained to the light of a microcalorimetric study performed by Muhler et al. on Au/ZnO [39]: adsorbed CO can react with removable lattice oxygen and form CO_2, thus creating oxygen vacancies the formation of which is favored at the Au/ZnO interface [5]. It could be therefore concluded that the creation of these oxygen vacancies at the Au-ZnO interface during CO adsorption modifies the electronic properties of gold, and leads to the formation of $Au^{\delta-}$ sites. However, this does not explain that the same phenomenon of growth of the low IR frequency band at the expense of the high frequency one was also observed in systems, such as Au on SiO_2 [38] on which oxygen vacancies are not expected to form. Bianchi et al. [40] proposed an alternative assignment to the band at 2070 cm^{-1} on spectra of Au/Al_2O_3; they assigned it to the formation of new Au^{0} adsorption sites resulting from gold nanoparticles restructuring under CO, as attested by a heat of CO adsorption different from the one corresponding to the band at 2100 cm^{-1}. Anyhow, whatever the attribution of the low frequency CO band, the important result to be drawn from Figure 9 is that the overall intensity of the spectra of the reduced Au/ZnO sample is much lower than that of the calcined one (Figure 9C). This is discussed in the next section.

One can also note that the baseline of the spectra of the calcined sample is flat at the beginning of CO adsorption, but becomes more and more tilted with time under CO (Figure 9A) whereas the baseline of the reduced sample is already tilted from the very beginning and does not change with time (Figure 9B); this has been already observed in a previous IR study of ZnO Kadox on which H_2 was adsorbed [41]. According to the authors, this is typical of radiation scattered by free electrons arising from their release from the conduction band.

6. Discussion

The formation of alloy-type nanoparticles during reduction of a noble metal supported on ZnO has been observed previously. For more than twenty years, the formation of Pd-Zn alloy in reduced Pd/ZnO has been assumed then proved [42-44]. It has been also reported for Pt, Rh and very recently for Au. The formation of Au-Zn alloy has been detected by Checa et al. in 2012 [45]. An Au/ZnO sample with 5 wt% Au prepared by deposition-precipitation with NaOH at pH 7 exhibited large Au^0 particles of 12 nm after reduction at 200°C and Au-Zn alloy particles of 14 nm after reduction at 400°C, with an XRD peak at 40.5°, close to the one observed in this study in DPU Au/ZnO (Figure 6) and in Impregnated Au/ZnO (Figure 7). The same year, Liu et al. [29] also identified the presence of a Au-Zn nanoalloy by EXAFS in an Au/ZnO (20 wt% Au) sample reduced at 300 °C.

Interestingly, Sarkany et al. [43] observed a decrease in the activity of hydrogenation of 1,3-butadiene over Pd/ZnO catalysts as the reduction temperature of the catalyst increased. This decrease of activity was accompanied by an increase in selectivity to butenes and a decrease in the *trans*/*cis*-2-butene ratio that they correlated to the formation of a Pd-Zn intermetallic phase that decreased the availability of the Pd adsorption sites. More recently, Tew et al [46] also reported that the formation of Pd_1Zn_1 alloy in Pd/ZnO (4.3 wt% Pd) reduced at 300 °C decreased the activity in hydrogenation of 1-pentyne, inhibited total hydrogenation and favoured the high selectivity to pentenes compared to a Pd/SiO_2 catalyst containing Pd^0 particles. They attributed the suppression of the total hydrogenation to changes in the electronic properties of Pd due to the formation of the PdZn alloy whose electronic structure is very similar to that of copper, and also to the concomitant isolation of the Pd active sites. In the case of gold catalysts, which are intrinsically highly selective to semi-hydrogenation of dienes, but much less active than Pd, the formation of the Au_1Zn_1 alloy strongly inhibits the activity (Figure 3A).

The two studies of Checa et al. [45] and of Liu et al. [29] mentioned above, reported lower catalytic activity in reactions of oxidation of glycerol and of CO, respectively, when Au/ZnO was reduced and exhibited AuZn alloy formation, which is also what we observed for CO oxidation (Figure 4). In Liu's paper, the detrimental effect of the reduction at 300 °C to the catalytic activity in CO oxidation was explained by both an electronic effect because of the negative charge bared on the gold surface particles (resulting from the presence of an IR CO band at 2048 cm^{-1}, in addition to one around 2100 cm^{-1} of CO adsorbed on Au^0) and a geometric effect due to the formation of AuZn alloy.

In addition to this, in the present work, we demonstrated the reversibility of the Au_1Zn_1 alloy formation as a calcination treatment restored the activity of gold in CO oxidation (Figure 4). This was also verified directly by XRD with the sample prepared by impregnation (Figure 7). One can note that the initial activity obtained after the first calcination treatment (Figure 4Ba) is not fully recovered after the second one (Figure 4Bc); this can be due to the fact that the sample has been submitted to three successive thermal treatments and reaction, that the sample deactivates with time, and the metal particles could have grown.

The fact that the frequency of the CO bands in the calcined (2107 and 2075 cm^{-1}) and reduced DPU Au/ZnO samples (2101 and 2071 cm^{-1}) (Figure 9) are comparable to those observed fin calcined (2107 and 2075 cm^{-1}) and reduced Au/TiO_2 samples (2101 and 2074 cm^{-1}) whose metallic phase is Au^0 after both treatments [47], is an indication that the electronic properties of the surface gold atoms are not altered by the formation of Au_1Zn_1 alloy. XPS did not show either any shift in the gold binding energy between the calcined and the reduced Au/ZnO samples (Figure 8). Besides, no shift in the Au binding energy was either detected by Liu et al [29] when they compared Au/ZnO reduced at 300 °C to Au/ZnO calcined at 300 °C. No shift was either visible in the XPS figure of Checa's paper [45] in which they compared an

Au/ZnO sample reduced at 400 °C (AuZn formation) to one reduced at 200 °C (Au°). The absence of Au BE shift was also observed in Au-Pd [48] and refs therein and in Au-Pt systems [49]: only Pd or Pt BE shifted, attesting for the existence of an electron transfer. In the present work, the Zn peaks that can correspond to Zn of the Au_1Zn_1 alloy are included into the overall Zn peaks that are predominantly related to the ZnO support, thus no information regarding possible electronic effect can be drawn from the XPS results. The much lower intensity of the ν_{CO} band in the IR spectra of reduced Au/ZnO compared to the one of oxidized Au/ZnO (Figure 9C) is probably related to the fact that less CO can adsorb on the gold surface sites of Au_1Zn_1 particles. This interpretation compares with an IR study on Pd/ZnO sample by van Bokhoven and coll. [50]. The spectrum of CO adsorbed on Pd/ZnO reduced at 350 °C, i.e. in the conditions where PdZn forms, was much less intense than the one obtained after Pd had been first reduced at RT These results are consistent with ours and with our interpretation that the decrease if CO adsorption sites can be due to alloy formation. We propose therefore that the formation of Au_1Zn_1 alloy induces a strong decrease in the number of surface gold sites, and especially those on which CO can adsorb, which are the low coordinated gold atoms, also considered as the active sites in most of the gold catalyzed reactions. This is consistent with the lower activity in CO oxidation observed over the reduced Au/ZnO catalyst than over the calcined one (Figure 4). These low coordinated gold sites are also considered as those involved in H_2 activation, which is the rate-limiting step of hydrogenation reactions [51-52].

Hence, the inhibition of the reaction of hydrogenation of butadiene when Au/ZnO is reduced, and Au_1Zn_1 nanoalloy forms, does not seem to result from a modification of the electronic properties of gold, or at least, we could not find evidence for it. So, it may rather be due to a geometric effect due to the presence of Zn atoms at the particle surface that inhibits or modifies the capability of adsorption and activation of H_2 and maybe also of butadiene. Another question that could be raised is whether Au_1Zn_1 could form in the calcined sample

during the reaction. Although, we did not focus specifically on this point, it has already been mentioned in Section 3.2 that the profile of concentrations as a function of the reaction temperature of calcined Au/ZnO (Figure 3B) looks very similar in shape and temperature to that of Au/TiO_2 or Au/Al_2O_3, so this does not support the hypothesis that Au_1Zn_1 could form in calcined Au/ZnO during the reaction.

7. Conclusion

In contrast to other gold/oxide systems such as Au/TiO_2, Au/Al_2O_3 that have been already studied in the reaction of selective hydrogenation of butadiene in excess of propene, a similarly prepared and H_2 activated Au/ZnO catalyst showed only a poor activity over the 25-300 °C reaction temperature range. By contrast, after activation in air, the sample exhibited a catalytic activity comparable to these reference samples. The same type of behaviour was observed for the CO oxidation reaction at room temperature, with a lower activity after activation under H_2 than under air. Three hypotheses were successively investigated, a support effect resulting from the formation of oxygen vacancies on ZnO surface at the interface with gold particles during the reduction treatment, the encapsulation of gold nanoparticles by reduced ZnO species during reduction and a change in particle structure or composition. It turned out that using high resolution XRD, it has been possible to show that after reduction, the metal particles consist of an Au_1Zn_1 alloy, and to attribute the inhibition of the catalytic activity to the formation of these Au_1Zn_1 nanoparticles. Further investigation of the surface properties of these particles by XPS and CO-DRIFTS and the comparison to those of Au^0 particles in calcined Au/ZnO, did not reveal changes in the electronic properties of the surface gold atoms. The inhibition of activity was attributed to a geometric effect, i.e., the formation of the Au_1Zn_1 alloy reducing the number of low coordination gold sites at the surface, as attested by CO-DRIFTS and inhibiting reactant adsorption, i.e., the adsorption sites of CO in

the case of CO oxidation and the adsorption/activation of H_2 in the case of the reaction of hydrogenation.

Acknowledgments

The authors acknowledge the French Agence Nationale de la Recherche (ANR) for financial support under reference ANR-08-EFC-01-01. They warmly thank Prof John Regalbuto and his PhD student Jadid Samad of the University of South Carolina for the HR-XRD measurements. They also thank Christophe Calers, engineer at LRS, for the XPS measurements.

Table 1: Comparison of Au/ZnO activated in air or hydrogen at 300 °C with Au/TiO_2 and Au/Al_2O_3 prepared by DPU and activated in hydrogen at 300 °C: measured gold loading, gold particle size and temperature for 100% butadiene conversion

Catalysts	Au loading (wt %)	Activation gas	Average gold particle size (nm)		$T_{100\%}$	Refs
			Arithmetic mean	Volumic mean		
Au/ZnO	1.0	H_2	2.1	3.0	-	This work
Au/ZnO	1.0	Air	1.6	2.2	180	This work
Au/TiO_2	1.1	H_2	1.7	2.2	180	[15]
Au/Al_2O_3	0.9	H_2	2.2	2.8	165	[15]

Figure captions:

Figure 1: TPR profile of the as-prepared Au/ZnO sample (a) and ZnO (b)

Figure 2: TEM images of gold particles in Au/ZnO sample (A) reduced in H_2 at 300°C; (B) calcined in air at 300°C and the corresponding histograms of size distribution

Figure 3: Evolution of the conversion and the selectivities in hydrogenation of butadiene over Au/ZnO (A) reduced in H_2 at 300°C; (B) calcined in air at 300°C; (C) over Au/ZnO reduced in H_2 at 300°C, cooled down to RT, and then exposed to air for 24 h at RT

Figure 4: Comparison of the catalytic activity in CO oxidation after different sequences of activation (A) reduced in H_2 at 300°C (a); reduced in H_2, CO oxidation then calcined in air at 300°C (b); (B) calcined in air at 300°C (a); calcined in air, CO oxidation then reduced in H_2 at 300°C (b); calcined in air, CO oxidation then reduced in H_2, CO oxidation then calcined in air at 300°C (c)

Figure 5: HRTEM images of gold particles in Au/ZnO sample (A) after reduction at 300 °C; (B) after calcination at 300 °C

Figure 6: High-resolution XRD patterns of Au/ZnO (a) after calcination at 300 °C (black); (b) after reduction at 300 °C (red)

Figure 7: Evolution of the XRD patterns of Au/ZnO prepared by impregnation (1wt% Au) then calcined at 500°C and reduced at 300°C, as a function of the temperature of a subsequent calcination treatment

Figure 8: XPS peak of Au $4f_{7/2}$ in Au/ZnO (a) after calcination at 300 °C (black); (b) after reduction at 300 °C (red)

Figure 9: DRIFT spectra of Au/ZnO obtained (A) after *in situ* calcination at 300 °C; (B) after *in situ* reduction at 300 °C; the samples were cooled down to RT in He, then CO (1%) in He was flowed during 2h30 and 3h, respectively; the spectra were recorded first every 2 min then 5 and finally 10 min; (C) comparison of the very first spectrum (C) and very last one (D) of each series (calcined sample: black spectra; reduced sample: red spectrum)

References

1. Hartadi, Y.; Widmann, D.; Behm, R. J., CO2 Hydrogenation to Methanol on Supported Au Catalysts under Moderate Reaction Conditions: Support and Particle Size Effects *ChemSusChem* **2015,** *8*, 456-465.
2. Ke, Y.-H.; X.-X. Qin; Liu, C.-L.; Yang, R.-Z.; Dong, W.-S., Oxidative esterification of ethylene glycol in methanol to form methyl glycolate over supported Au catalysts *Catal. Sci. Technol.* **2014,** *4*, 3141-3150.
3. Wu, H.; L. Wang; Zhang, J.; Shen, Z.; Zhao, J., Catalytic oxidation of benzene, toluene and p-xylene over colloidal gold supported on zinc oxide catalyst *Catal.Comm.* **2011,** *12*, 859-865.
4. Boucher, M. B.; Yi, N.; Gittleson, F.; Zugic, B.; Saltsburg, H.; Flytzani-Stephanopoulos, M., Hydrogen production from methanol over gold supported on ZnO and CeO2 nanoshapes *J. Phys. Chem. C* **2011,** *115*, 1261-1268.
5. Strunk, J.; Kahler, K.; Xia, X.; Comotti, M.; Schuth, F.; Reinecke, T.; Muhler, M., Au/ZnO as catalyst for methanol synthesis: The role of oxygen vacancies *Appl. Catal A: General* **2009,** *359* 121–128.
6. Carabineiro, S. A. C.; Machado, B. F.; Bacsa, R. R.; Serp, P.; Drazic, G.; Faria, J. L.; Figueiredo, J. L., Catalytic performance of Au/ZnO nanocatalysts for CO oxidation. *J. Catal.* **2010,** *273*, 191-198.
7. Carley, A. F.; Morgan, D. J.; Song, N.; Roberts, M. W.; Taylor, S. H.; Bartley, J. K.; Willock, D. J.; Howard, K. L.; Hutchings, G. J., CO bond cleavage on supported nano-gold during low temperature oxidation *Phys. Chem. Chem. Phys.* **2011,** *13*, 2528-2538.
8. Noei, H.; Birkner, A.; Merz, K.; Muhler, M.; Wang, Y., Probing the Mechanism of Low-Temperature CO Oxidation on Au/ZnO Catalysts by Vibrational Spectroscopy *J. Phys. Chem. C* **2012,** *116*, 11181−11188.
9. Naknam, P.; Luengnaruemitchai, A.; Wongkasemjit, S., Preferential CO oxidation over Au/ZnO and Au/ZnO-Fe2O3 catalysts prepared by photodeposition. *Intern. J. Hydr. Ener.* **2009,** *34*, 9838-9846.
10. Dulnee, S.; Luengnaruemitchai, A.; Wanchanthuek, R., Activity of Au/ZnO catalysts prepared by photo-deposition for the preferential CO oxidation in a H2-rich gas *Intern. J. Hydr. Ener.* **2014,** *39*, 6443-6453.
11. Chen, P. K.; Lee, G. J.; Davies, S. H.; Masten, S. J.; Amutha, R.; Wu, J. J., Hydrothermal synthesis of coral-like Au/ZnO catalyst and photocatalytic degradation of Orange II dye *Mater. Res. Bull.* **2013,** *48*, 2375-2382.
12. Mondal, C.; Pal, J.; Ganguly, M.; Sinha, A. K.; Jana, J.; Pal, T., A one pot synthesis of Au-ZnO nanocomposites for plasmon-enhanced sunlight driven photocatalytic activity. *New J. Chem.* **2014,** *38*, 2999-3005.
13. Chamjangali, M.; Bagherian, G.; Bahramian, B.; Fahimi, R. B., Synthesis and application of multiple rods gold-zinc oxide nanostructures in the photocatalytic degradation of methyl orange *Intern. J. Env. Sci. Technol.* **2015,** *12*, 151-160.
14. Yu, H.; Ming, H.; Zhang, H.; Li, H.; Pan, K.; Liu, Y.; Wang, F.; Gong, J.; Kang, Z., Au/ZnO nanocomposites: Facile fabrication and enhanced photocatalytic activity for degradation of benzene *Mater. Chem. Phys.* **2012,** *137*, 113-117.
15. Hugon, A.; Delannoy, L.; Louis, C., Supported gold catalysts for selective hydrogenation of 1,3-butadiene in the presence of an excess of alkenes. *Gold Bull.* **2008,** *41*, 127-138.

16. Hugon, A.; Delannoy, L.; Louis, C., Influence of the Reactant Concentration in Selective Hydrogenation of 1,3-Butadiene Over Supported Gold under Alkene Rich Conditions: A consideration of reaction mechanism. *Gold Bull.* **2009,** *42* 310-320.
17. Hugon, A.; Delannoy, L.; Krafft, J.-M.; Louis, C., Supported Gold-Palladium Catalysts for Selective Hydrogenation of 1,3 Butadiene in an Excess of Propene. *J. Phys. Chem. C* **2010,** *114*, 10823–10835.
18. Zanella, R.; Giorgio, S.; Henry, C. R.; Louis, C., D350 Alternative methods for the preparation of gold nanoparticles supported on TiO2. *J. Phys. Chem. B* **2002,** *106* (31), 7634-7642.
19. Zanella, R.; Delannoy, L.; Louis, C., D531 Mechanism of Deposition of Gold Precursors onto TiO2 during the Preparation by Deposition-Precipitation with NaOH and with Urea and by Cation Adsorption. *Appl. Catal. A* **2005,** *291*, 62-72.
20. Plzak, V.; Garche, J.; Behm, R. J., Au/MeOx catalysts in gas processing for PEM Fuel Cells: An overview of the resultst at ZSW/Uni-Ulm. *Eur. Fuel Cell News* **2003,** *10*, 16-20.
21. Hugon, A.; El Kolli, N.; Louis, C., Advances in the preparation of supported gold catalysts: Mechanism of deposition, simplification of the procedures and relevance of the elimination of chlorine. *J. Catal.* **2010,** *274*, 239-250.
22. Chen, Y.-W.; Lee, D.-S.; Chen, H.-J., Preferential oxidation of CO in H2 stream on Au/ZnO/TiO2 catalysts. *Intern. J. Hydr. Ener.* **2012,** *37*, 15140-15155.
23. Kundu, P.; Singhania, N.; Madras, G.; Ravishankar, N., ZnO–Au nanohybrids by rapid microwave-assisted synthesis for CO oxidation. *Dalton Trans.* **2012,** *41*, 8762–8766.
24. Boucher, M. B.; Goergen, S.; Yi, N.; Flytzani-Stephanopoulos, M., 'Shape effects' in metal oxide supported nanoscale gold catalysts. *Phys. Chem. Chem. Phys.* **2011,** *13*, 2517–2527
25. El Kolli, N.; Delannoy, L.; Louis, C., Bimetallic Au–Pd catalysts for selective hydrogenation of butadiene: Influence of the preparation method on catalytic properties. *J. Catal.* **2013,** *297* 79–92.
26. Boccuzzi, F.; Morterra, C.; Scala, R.; Zecchina, A., Infrared Spectrum of Microcrystalline Zinc Oxide- Electronic and Vibrational Contributions under Different Temperature and Environmental Conditions. *J. Chem. Soc., Faraday Trans. 2* **1981,** *77*, 2059-2066.
27. Drouilly, C.; Krafft, J. M.; Averseng, F.; Casale, S.; Bazer-Bachi, D.; Chizallet, C.; Lecocq, V.; Vezin, H.; Lauron-Pernot, H.; Costentin, G., ZnO Oxygen Vacancies Formation and Filling Followed by in Situ Photoluminescence and in Situ EPR. *J. Phys. Chem. C* **2012,** *116*, 21297-21307
28. Tauster, S. J.; Fung, S. C.; Garten, R. L., Strong metal-support interactions. Group 8 noble metals supported on titanium dioxide. *J. Am. Chem. Soc.* **1978,** *100*, 170.
29. Liu, X.; Liu, M.-H.; Luo, Y.-C.; Mou, C.-Y.; Lin, S. D.; Cheng, H.; Chen, J.-M.; Lee, J.-F.; Lin, T.-S., Strong Metal−Support Interactions between Gold Nanoparticles and ZnO Nanorods in CO Oxidation. *J. Am. Chem. Soc.* **2012,** *134*, 10251−10258.
30. Derrouiche, S.; Lauron-Pernot, H.; Louis, C., Synthesis and treatment parameters for controlling metal particle size and composition in Cu/ZnO materials - First evidence of Cu3Zn alloy formation. *Chem. Mater.* **2012,** *24*, 2282−2291.
31. Zwijnenburg, A.; Goossens, A.; Sloof, W. G.; Crajé, M. W. J.; van der Kraan, A. M.; Jos de Jongh, L.; Makkee, M.; Moulijn, J. A., D369 XPS and Mössbauer Characterization of Au/TiO2 Propene Epoxidation Catalysts. *J. Phys. Chem. B* **2002,** *106* (38), 9853-9862.
32. Radnik, J.; Mohr, C.; Claus, P., D474 On the origin of binding energy shifts of core levels of supported gold nanoparticles and dependence of pretreatment and material syntesis. *Phys. Chem. Chem. Phys.* **2003,** *5*, 172-177.

33. Arii, S.; Morfin, F.; Renouprez, A. J.; Rousset, J. L., D501 oxidation of CO on gold supported catalyts prepared by laser vaporization; direct evidence of support contribution. *J. Am. Chem. Soc.* **2004,** *126*, 1199-1205.
34. Kruse, N.; Chenakin, S., XPS characterization of Au/TiO2 catalysts: Binding energy assessment and irradiation effects. *Appl. Catal. A: General* **2011,** *391*, 367–376.
35. Moulder, J. F.; Stickle, W. F.; Sobol, P. E.; Bomben, K. D., Handbook of X-ray Photoelectron Spectroscopy,. **1992**.
36. Boccuzzi, F.; Chiorino, A.; Manzoli, M.; Andreeva, D.; Tabakova, T., D92 FTIR study of the low-temperature water-gas shift reaction on Au/Fe2O3 and Au/TiO2 catalysts. *J. Catal.* **1999,** *188*, 176-185.
37. Mihaylov, M.; Knözinger, H.; Hadjiivanov, K.; Gates, B. C., Characterization of the Oxidation States of Supported Gold Species by IR Spectroscopy of Adsorbed CO. *Chem. Ing. Technik* **2007,** *79*, 795-806.
38. Chakarova, K.; Mihaylov, M.; Ivanova, S.; Centeno, M. A.; Hadjiivanov, K., Well-Defined Negatively Charged Gold Carbonyls on Au/SiO2. *J. Phys. Chem. C* **2011,** *115* 21273-21282.
39. Xia, X.; Strunk, J.; Busser, W.; Comotti, M.; Schuth, F.; Muhler, M., Thermodynamics and Kinetics of the Adsorption of Carbon Monoxide on Supported Gold Catalysts Probed by Static Adsorption Microcalorimetry: The Role of the Support. *J. Phys. Chem. C* **2009,** *113*, 9328–9335.
40. Roze, E.; Gravejat, P.; Quinet, E.; Rousset, J. L.; Bianchi, D., Impact of the Reconstruction of Gold Particles on the Heats of Adsorption of Linear CO Species Adsorbed on the Au Sites of a 1% Au/Al2O3 Catalyst. *J. Phys. Chem C.* **2009,** *113*, 1037 - 1045.
41. Ghiotti, G.; Chiorino, A.; Boccuzzi, F., Surface chemistry and electronic effects of H2 (D2) on two different microcrystalline ZnO powders. *Surf. Sci.* **1993,** *287-288*, 228-234.
42. Hong, C.-T.; Yeh, C.-T.; Yu, F.-H., Effect of reduction and oxidation treatments on palladium/zinc oxide catalysts. *Appl. Catal.* **1989,** *48* 385.
43. Sarkany, A.; Zsoldos, Z.; Furlong, B.; Hightower, J. W.; Guczi, L., Hydrogenation of 1-butene and 1,3-butadiene mixtures over Pd/ZnO catalysts. *J. Catal.* **1993** *141*, 566-582.
44. Zsoldos, Z.; Sarkany, A.; Guczi, L., XPS evidence of alloying in Pd/ZnO catalysts. *J. Catal.* **1994,** *145* 235.
45. Checa, M.; Auneau, F.; Hidalgo-Carrillo, J.; Marinas, A.; Marinas, J. M.; Pinel, C.; Urbano, F. J., Catal. Today. **2012,** *196* 91-100.
46. Tew, M. W.; Emerich, H.; van Bokhoven, J. A., Formation and Characterization of PdZn Alloy: A Very Selective Catalyst for Alkyne Semihydrogenation. *J. Phys. Chem. C* **2011,** *115*, 8457–8465.
47. Sandoval, A.; Louis, C.; Zanella, R., Improved activity and stability in CO oxidation of bimetallic Au–Cu/TiO2 catalysts prepared by deposition–precipitation with urea. *Appl. Catal. B* **2013,** *140-141*, 363-377.
48. Giorgio, S.; Mattei, J. G.; Henry, C. R.; Kolli, N. E.; Delannoy, L.; Louis, C., Surface Segregation of Pd under CO oxidation reaction in AuPd nanoalloys supported on TiO2 in situ observed by ETEM and DRIFTS *ChemCatChem* **2013,** *5*, 2707-2716.
49. Doherty, R. P.; Krafft, J.-M.; Méthivier, C.; Casale, S.; Remita, H.; Louis, C.; Thomas, C., On the promoting effect of Au on CO oxidation kinetics of Au-Pt bimetallic nanoparticles supported on SiO2: an electronic effect? *J. Catal.* **2012,** *287*, 102-113.
50. Fottinger, K.; van Bokhoven, J. A.; Nachtegaal, M.; Rupprechter, G., Dynamic Structure of a Working Methanol Steam Reforming Catalyst: In Situ Quick-EXAFS on Pd/ZnO Nanoparticles. *J. Phys. Chem. Lett.* **2011,** *2*, 428-433.

51. Zanella, R.; Louis, C.; Giorgio, S.; Touroude, R., D483 Hydrogenation of crotonaldehyde by Nanoparticles of gold supported on TiO2 prepared by Deposition-precipitationwith NaOH and Urea. *J. Catal.* **2004,** *223*, 328-339.
52. Bus, E.; Miller, J. T.; van Bokhoven, J. A., D852 Hydrogen Chemisorption on Al2O3-Supported Gold Catalysts. *J. Phys. Chem. B* **2005,** *109*, 14581-14587.

Figure 1

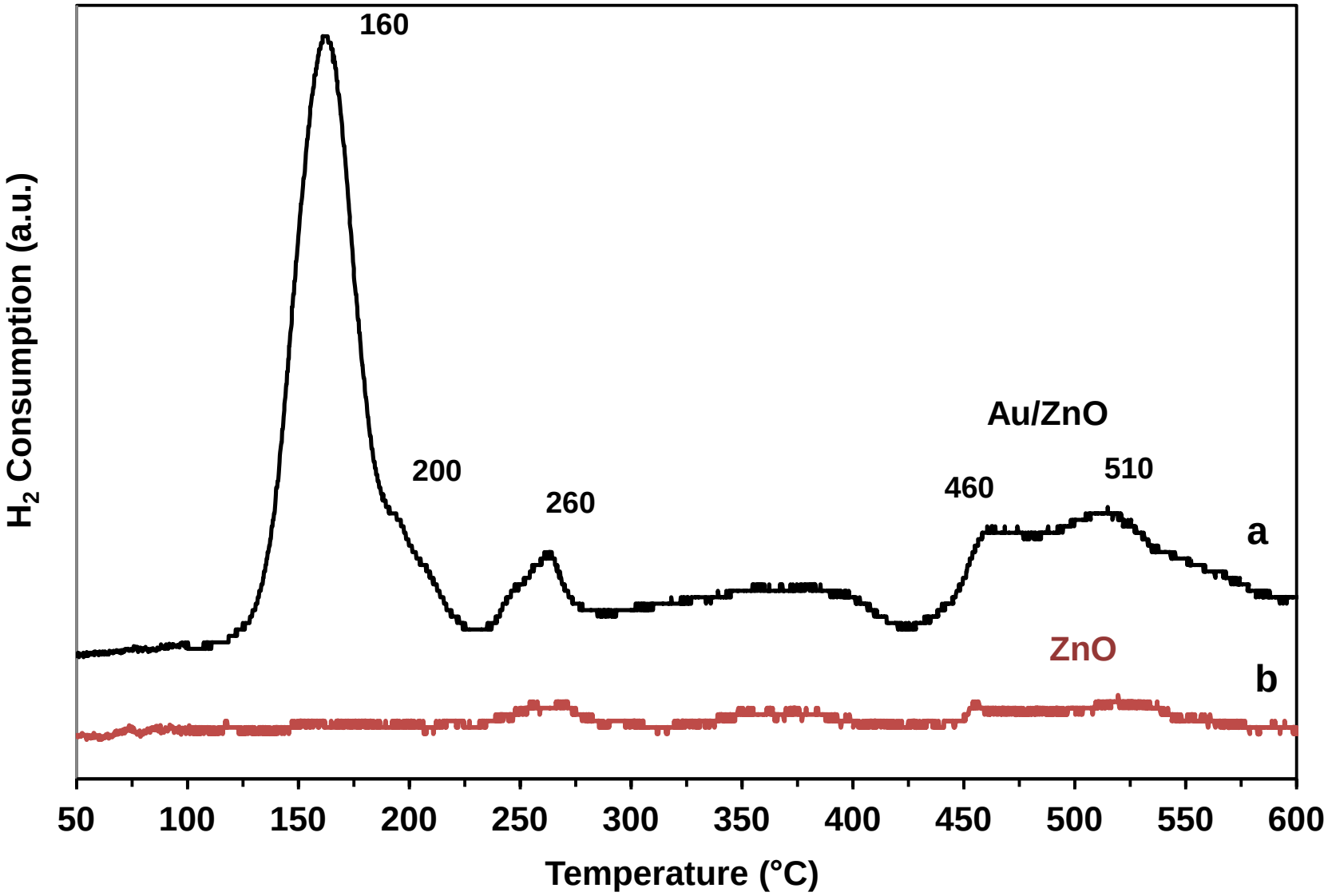
160
200
260
460
510
Au/ZnO
a
ZnO
b
H2 Consumption (a.u.)
50
100
150
200
250
300
350
400
450
500
550
600
Temperature (°C)

Figure 2

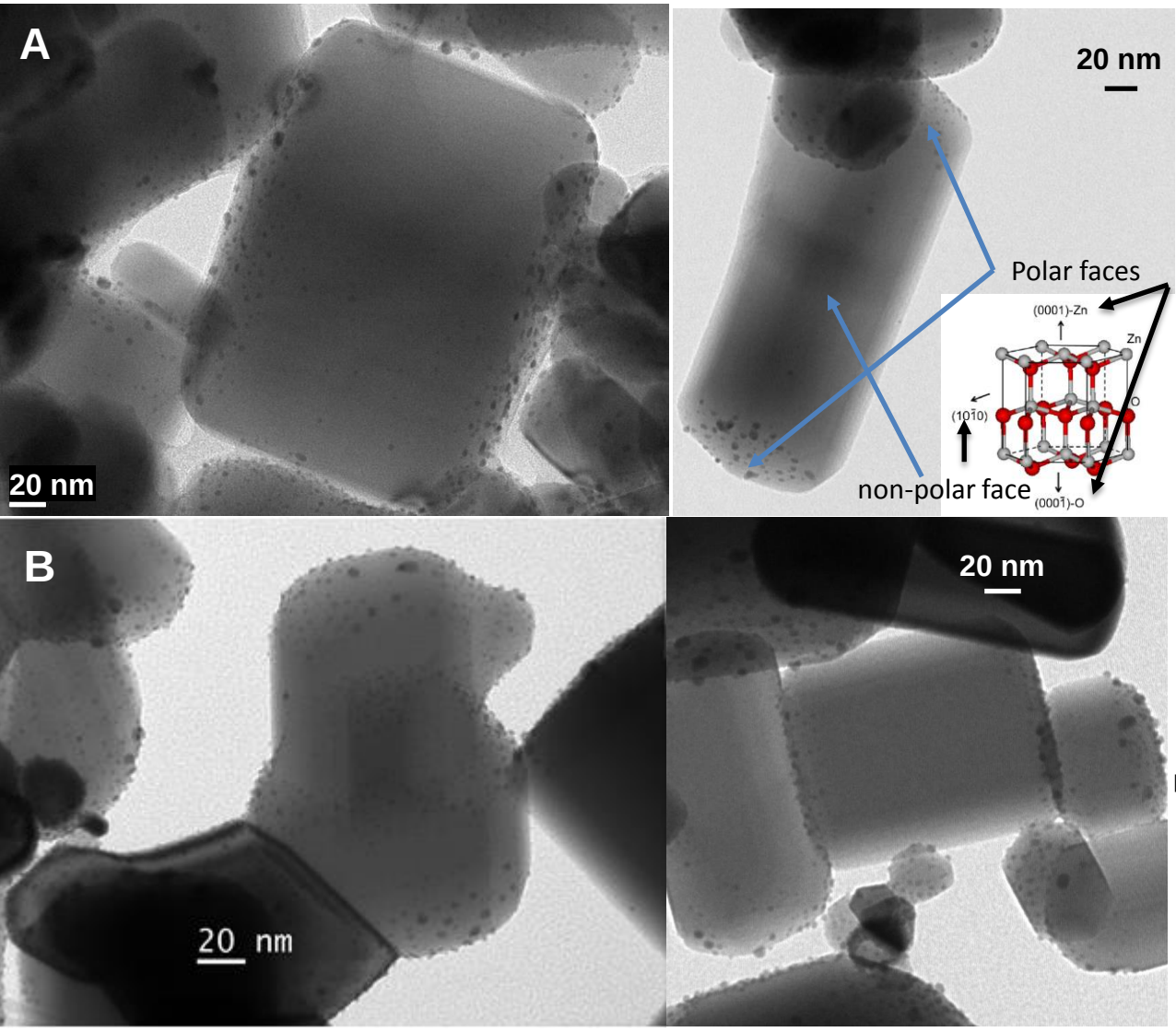
A
20 nm
20 nm
Polar faces
non-polar face
(0001)-Zn
Zn
O
(10$\bar{1}$0)
(000$\bar{1}$)-O
B
20 nm
20 nm
Frequency
0 1 2 3 4 5 6 7 8
Size (nm)
Frequency
0 1 2 3 4 5 6 7 8
Size (nm)

Figure 3A

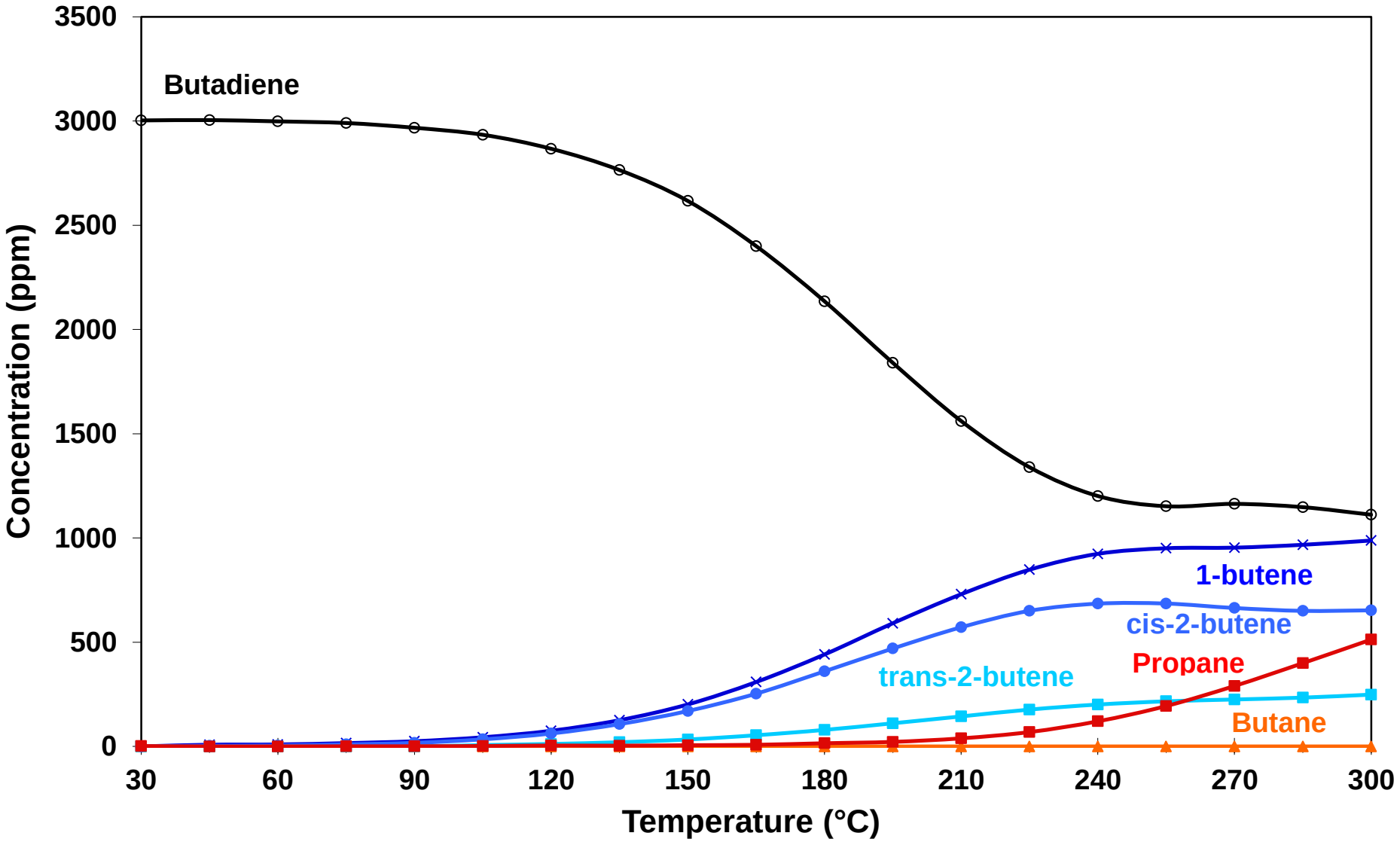
Butadiene
1-butene
cis-2-butene
trans-2-butene
Propane
Butane
Concentration (ppm)
Temperature (°C)
3500
3000
2500
2000
1500
1000
500
0
30
60
90
120
150
180
210
240
270
300

Figure 3B

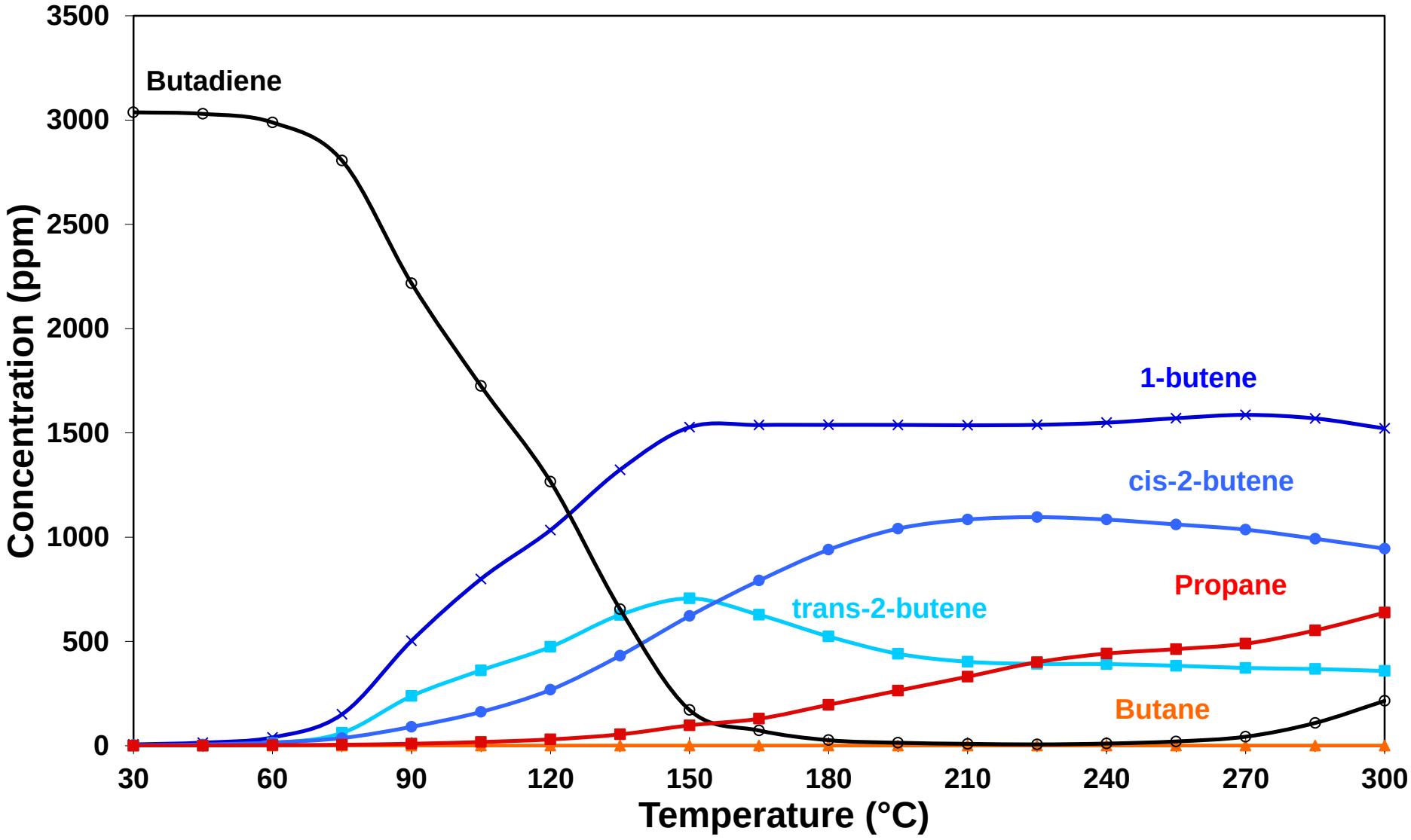
Butadiene
1-butene
cis-2-butene
trans-2-butene
Propane
Butane
Concentration (ppm)
Temperature (°C)
3500
3000
2500
2000
1500
1000
500
0
30
60
90
120
150
180
210
240
270
300

Figure 3C

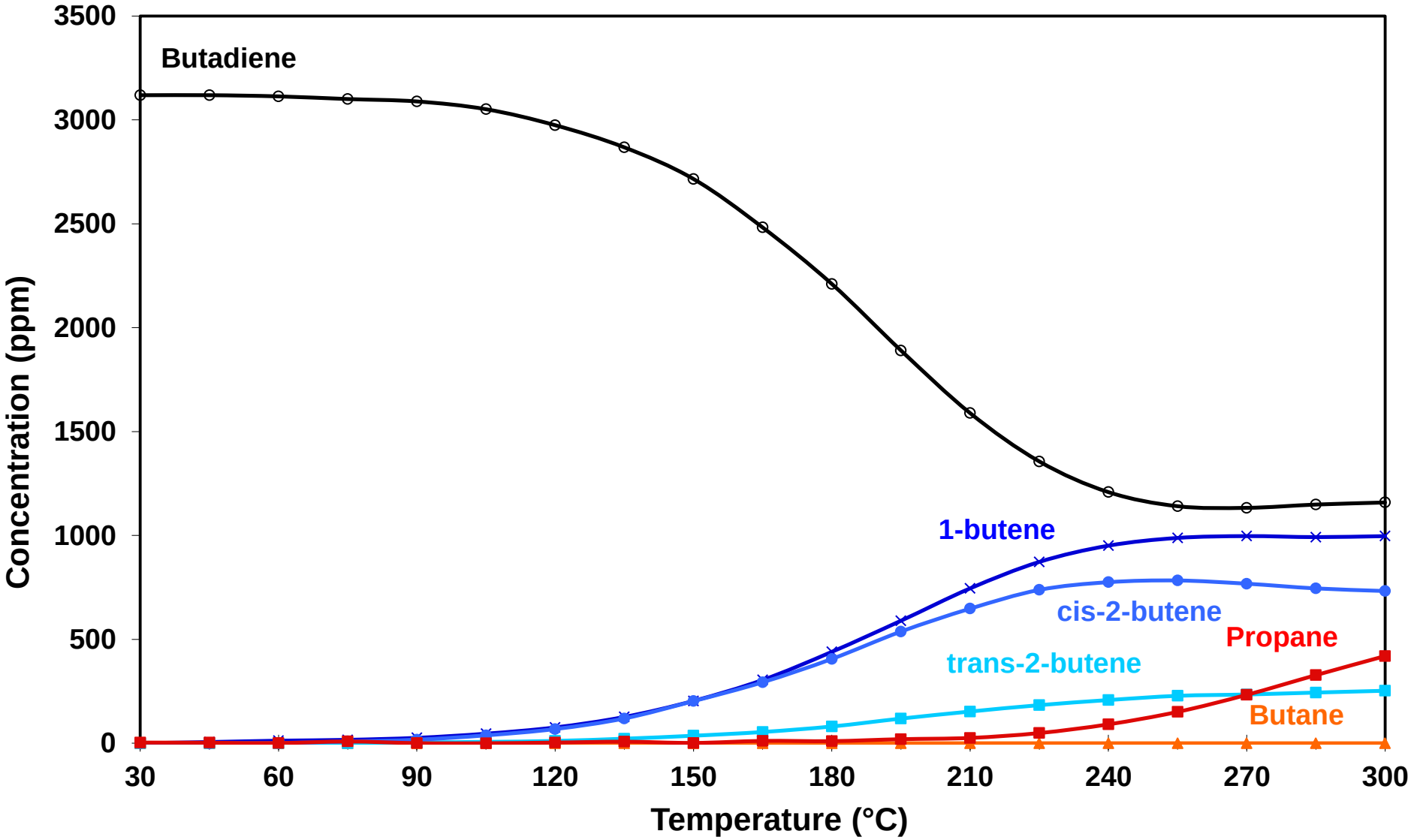
Butadiene
1-butene
cis-2-butene
trans-2-butene
Propane
Butane
Concentration (ppm)
Temperature (°C)
3500
3000
2500
2000
1500
1000
500
0
30
60
90
120
150
180
210
240
270
300

Figure 4

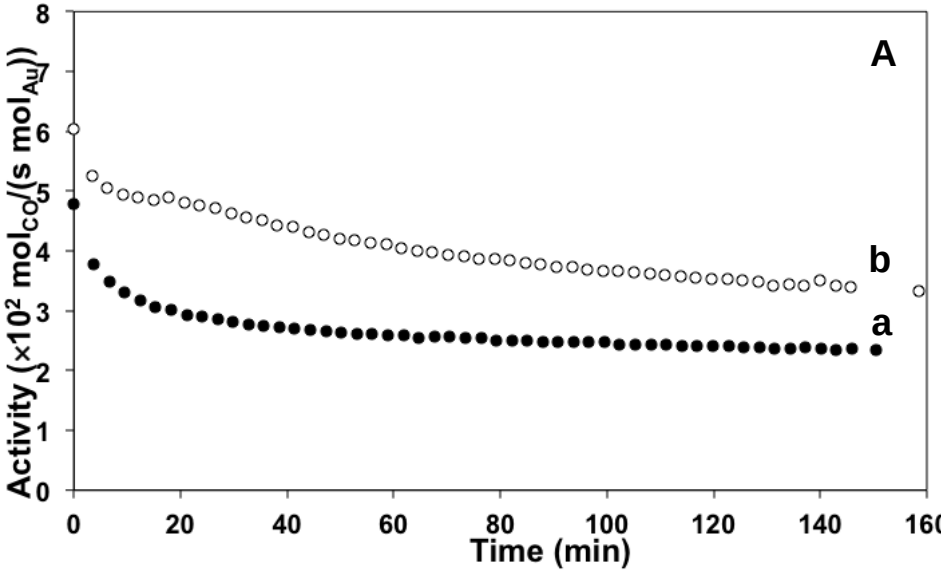
A
b
a
Activity (×10² mol$_{CO}$/(s mol$_{Au}$))
Time (min)
0
20
40
60
80
100
120
140
160
1
2
3
4
5
6
7
8

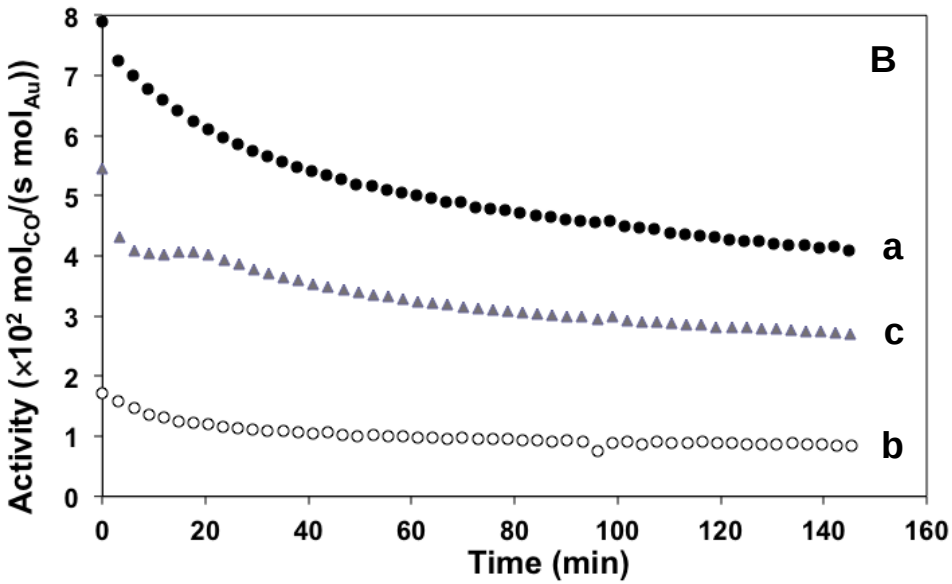
B
a
c
b
Activity (×10² mol$_{CO}$/(s mol$_{Au}$))
Time (min)
0
20
40
60
80
100
120
140
160
1
2
3
4
5
6
7
8

Figure 5

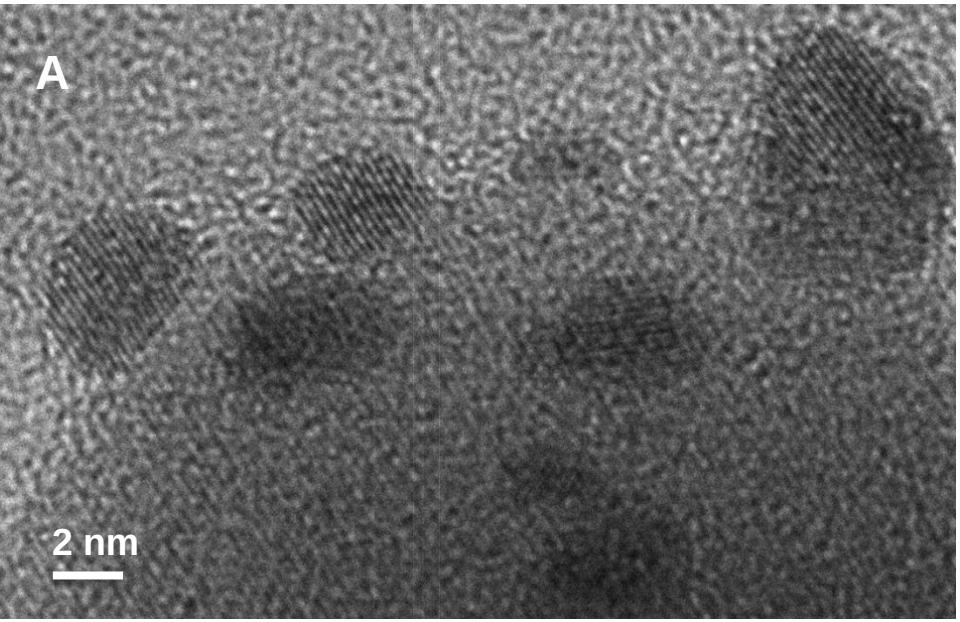

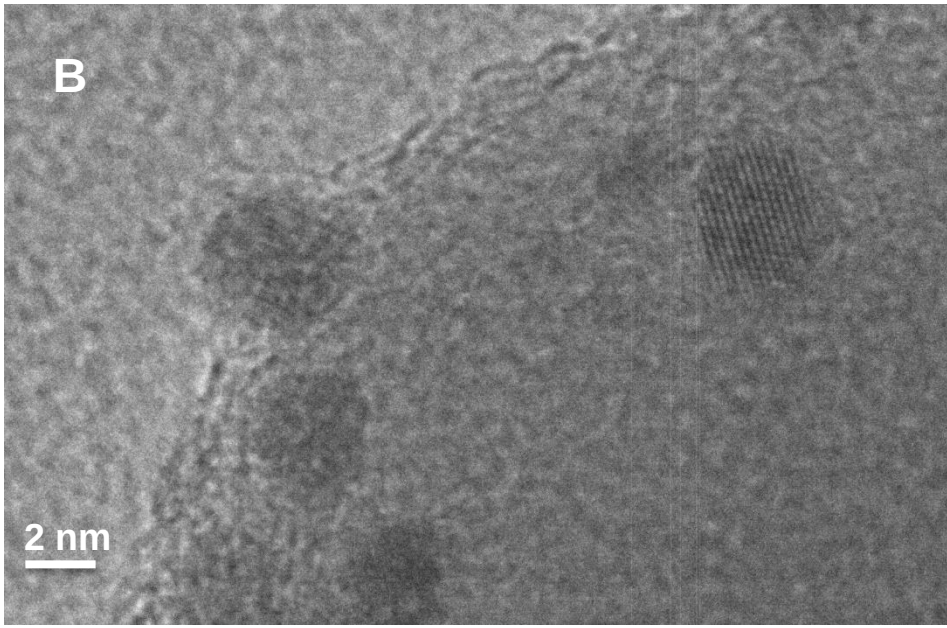

Figure 6

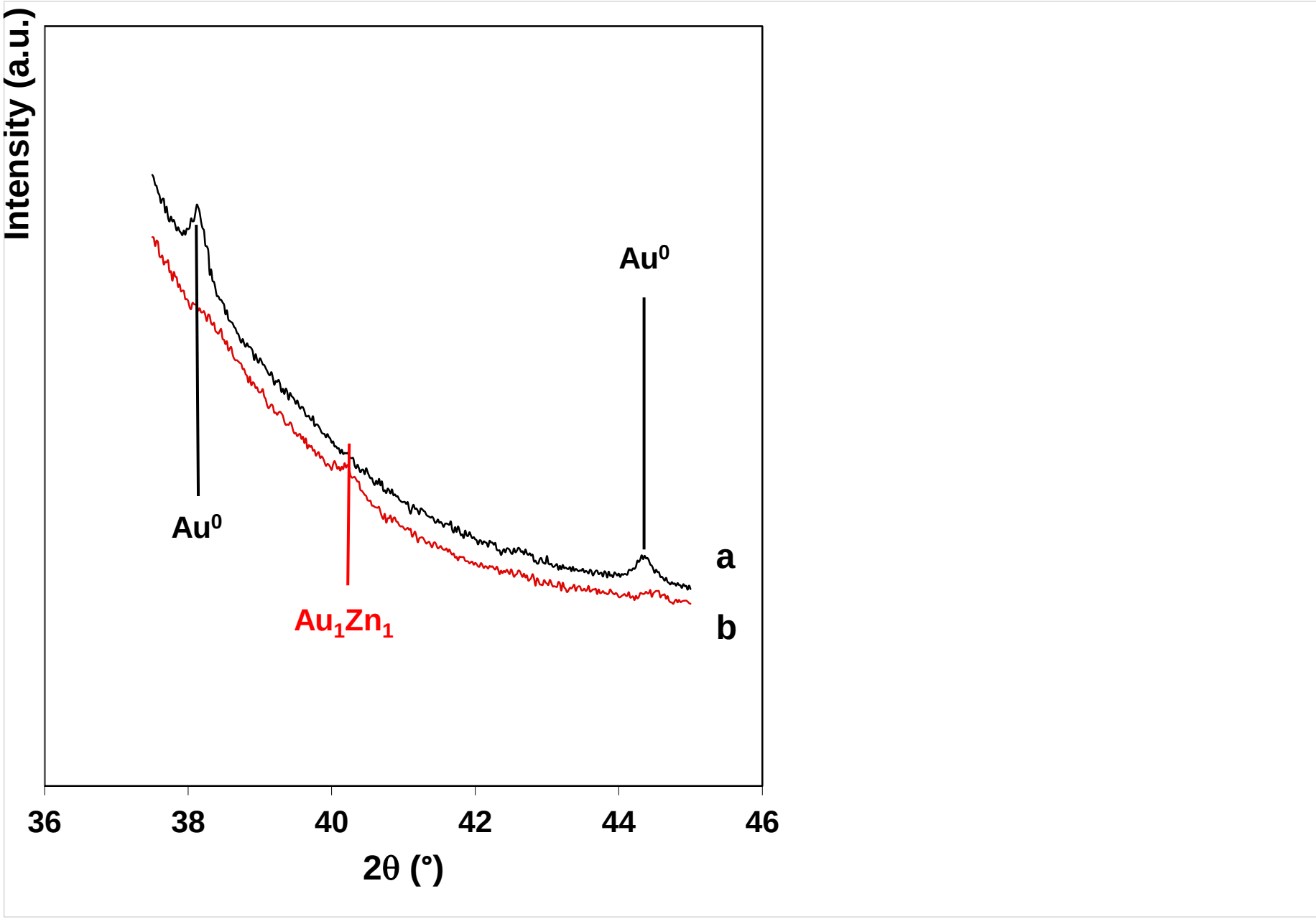

Figure 7

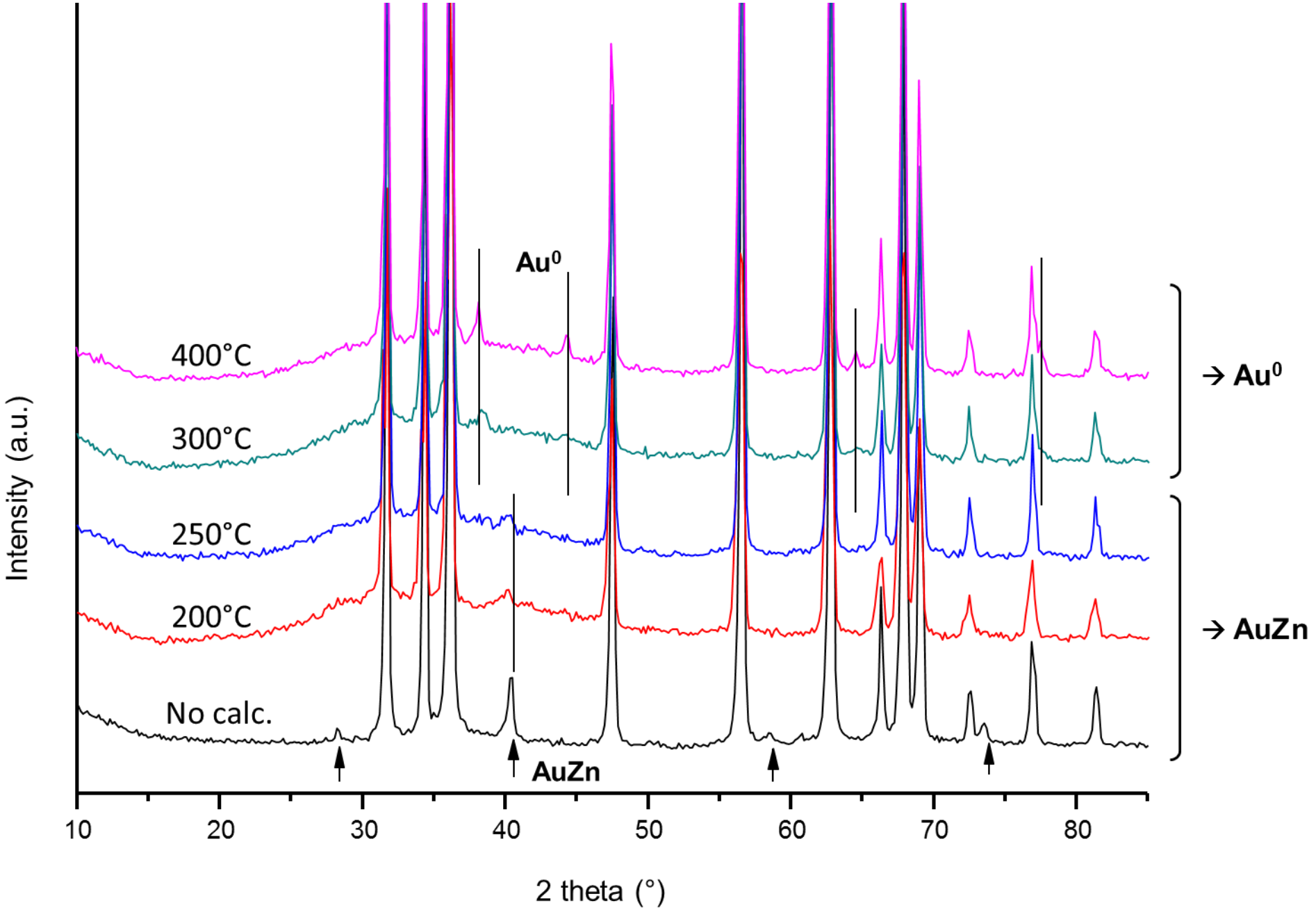
Au⁰
400°C
300°C
250°C
200°C
No calc.
AuZn
→ Au⁰
→ AuZn
Intensity (a.u.)
10
20
30
40
50
60
70
80
2 theta (°)

Figure 8

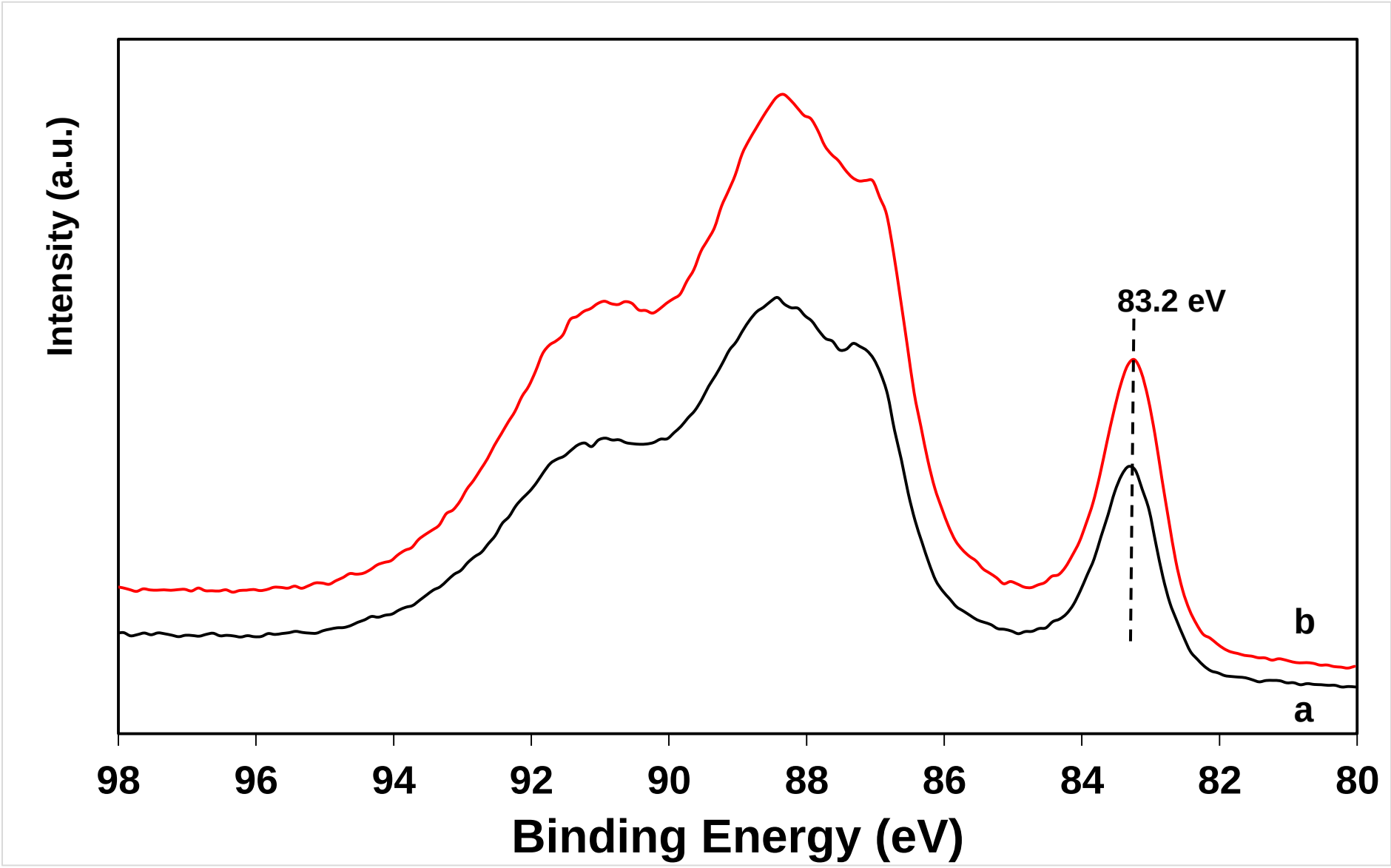
Intensity (a.u.)
83.2 eV
b
a
98
96
94
92
90
88
86
84
82
80
Binding Energy (eV)

Figure 9

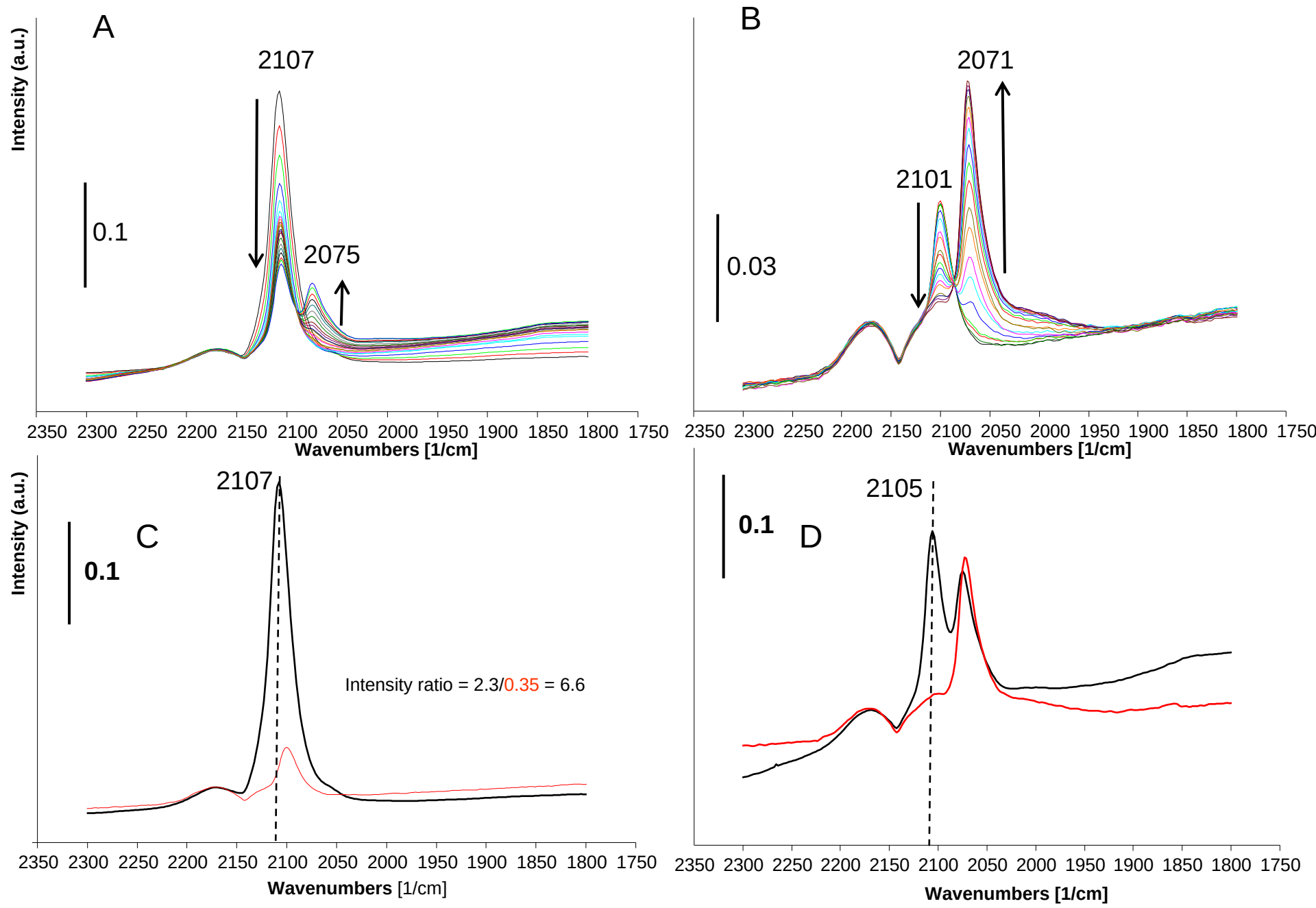
A
2107
2075
0.1
Intensity (a.u.)
2350 2300 2250 2200 2150 2100 2050 2000 1950 1900 1850 1800 1750
Wavenumbers [1/cm]
B
2071
2101
0.03
2350 2300 2250 2200 2150 2100 2050 2000 1950 1900 1850 1800 1750
Wavenumbers [1/cm]
C
2107
0.1
Intensity (a.u.)
Intensity ratio = 2.3/0.35 = 6.6
2350 2300 2250 2200 2150 2100 2050 2000 1950 1900 1850 1800 1750
Wavenumbers [1/cm]
D
2105
0.1
2350 2300 2250 2200 2150 2100 2050 2000 1950 1900 1850 1800 1750
Wavenumbers [1/cm]